Adsorbate–adsorbate interactions for PF3 chemisorbed on Pt(111)

Vijay K. Agrawal and Michael Trenary

Citation: The Journal of Chemical Physics **95**, 6962 (1991); doi: 10.1063/1.461507
View online: http://dx.doi.org/10.1063/1.461507
View Table of Contents: http://scitation.aip.org/content/aip/journal/jcp/95/9?ver=pdfcov
Published by the AIP Publishing

Adsorbate–adsorbate interactions for PF_3 chemisorbed on Pt(111)

Vijay K. Agrawal and Michael Trenary
Department of Chemistry, University of Illinois, Box 4348, Chicago, Illinois 60680

(Received 24 May 1991; accepted 22 July 1991)

To gain a better understanding of adsorbate–adsorbate interactions for chemisorbed polyatomic molecules we have measured the coverage and temperature dependence of the PF_3 symmetric bend and P–F symmetric stretch fundamentals of PF_3 chemisorbed on Pt(111). The two bands exhibit distinctly different responses to lateral interactions. The P–F stretch shifts from 901 to 951 cm^{-1} with increasing coverage and at intermediate coverages splits into two components separated by 5–13 cm^{-1} with a relative intensity which is strongly temperature dependent. By contrast, the symmetric bend shifts from 541 to 562 cm^{-1} and remains as a single band under all conditions. The symmetric bend displays only a slight asymmetry under conditions where the P–F stretch is split into two components. The different behavior of the two bands along with other considerations indicate that both coupling and chemical shifts determine the P–F stretch frequency for PF_3 chemisorbed on Pt(111).

INTRODUCTION

Adsorbate–adsorbate interactions determine the two-dimensional structures assumed by molecules chemisorbed on metal surfaces. A given adsorbate/substrate system can display a variety of both ordered and disordered phases which depend on both coverage and temperature.[1] As a consequence, the local environment for a given molecule in terms of the number and distances of neighboring adsorbate molecules can be highly varied. Furthermore, the adsorbate environment is often a strong function of both temperature and coverage even when only one type of substrate site is occupied. Because the much stronger adsorbate-substrate interactions tend to dominate the energetics of chemisorption, only a few experimental techniques are sensitive to the much weaker adsorbate–adsorbate interactions. Low-energy electron diffraction (LEED) is sensitive to long-range order and has traditionally been the most important tool for characterizing overlayer structures. However, LEED provides little information on molecules which are not part of an ordered structure. With the high resolution obtainable with infrared reflection absorption spectroscopy, it is observed that adsorbate vibrational frequencies are sensitive to the local environment. Furthermore, the relationship between the spectra and the environment does not depend on the presence of long-range order. Thus new insights on adsorbate structure and adsorbate phase transitions can potentially be gained through precise measurements of adsorbate vibrational spectra as a function of coverage and temperature. In this paper we make a detailed analysis of the coverage and temperature dependence of the symmetric P–F stretch and symmetric PF_3 bend fundamentals for PF_3 chemisorbed on Pt(111) as observed with Fourier transform infrared reflection absorption spectroscopy (FT-IRAS).

In two previous FT-IRAS studies we have reported on the basic features of the PF_3/Pt(111) system.[2,3] At a full coverage of 0.33 ML (monolayer) we observe the symmetric P–F stretch at 951 cm^{-1} and the symmetric PF_3 bend at 562 cm^{-1}. At this coverage both bands are unusually narrow with widths (FWHM) of 1.3 and 0.7 cm^{-1}, respectively. At intermediate coverages the P–F symmetric stretch band shows two components separated by 5–10 cm^{-1} whose relative intensity shows strong variations with both coverage and temperature. Concurrent LEED observations revealed the development of a $(\sqrt{3}\times\sqrt{3})R$ 30° overlayer pattern at coverages less than the 0.33 ML associated with the complete overlayer structure. This suggested that the variations in the P–F band shape was associated with the growth of two-dimensional islands of PF_3 in a $(\sqrt{3}\times\sqrt{3})R$ 30° ordered structure. We assigned the higher-frequency component to molecules within ordered islands and the lower-frequency component to molecules in a lower density disordered phase. This simple lattice-gas model offered a compelling qualitative explanation for our observations.

The interpretation of our IR data in terms of island formation was further supported by the strong parallels which exist between the PF_3/Pt(111) and CO/Ru(001) systems. In the latter case, formation of ordered islands of the $(\sqrt{3}\times\sqrt{3})R$ 30° structure has been extensively studied with LEED (Refs. 4, 5, and 6) and IR (Ref. 7). Just as we observe two components of the P–F stretch which change in relative intensity with both coverage and temperature, so did Pfnür *et al.*[7] observe the analogous behavior for two components of the C–O stretch. The simple lattice-gas model involves a large repulsive interaction, J_1, for nearest-neighbor sites and a smaller attractive interaction, J_2, for next-nearest-neighbor sites. For the CO/Ru(001) system, careful thermal desorption experiments[8] yielded $J_1 = 12$ kJ/mol and $J_2 = -3$ kJ/mol. It is important to note that the thermal desorption traces of CO from Ru(001) display shifts to lower temperature and the development of a lower temperature shoulder with increasing coverage just as we observe in thermal desorption of PF_3 from Pt(111). Models[9] of thermal desorption which account for lateral interactions by allowing the activation energy, but not the preexponential, to vary with coverage, predict a shift of the desorption peak to higher temperatures in the presence of attractive interac-

 0021-9606/91/216962-10$03.00

tions. However, activation energies and preexponentials are not independent but are related by the compensation effect.[10] When the compensation effect is considered, decreasing peak temperatures with increasing coverage can occur in the presence of attractive lateral interactions.[10] Thus, the TPD (temperature programmed desorption) traces observed for PF_3/Pt(111) and CO/Ru(001) are completely consistent with a small attractive next-nearest-neighbor interaction in addition to a repulsive nearest-neighbor interaction.

The high quality and apparent simplicity of our IR data for PF_3 on Pt(111) suggest that a more quantitative analysis could provide additional details on the island formation phenomena and the lateral interactions involved. Ideally, such analysis could lead to expanded use of high-resolution adsorbate vibrational spectroscopy for the study of phenomena which has previously been the sole domain of diffraction techniques. The potential for applying IRAS for studying such phenomena has been suggested in numerous studies of CO chemisorbed on transition-metal surfaces[11,12] and has recently been reemphasized by Ryberg in a study of CO on Pt(111).[13] While there has been considerable precedent for using IRAS to characterize lateral interactions for chemisorbed diatomics, there has been comparatively little work on polyatomic molecules where two or more intramolecular vibrational modes can be studied. As in the present study of PF_3 on Pt(111), the ability to monitor the fundamental band of more than one intramolecular vibrational mode can provide additional insights into adsorbate–adsorbate interactions.

The chemisorption of PF_3 on metal surfaces has been the subject of several previous surface-science studies.[14–23] Nitschké *et al.*[14] used ultraviolet photoelectron spectroscopy to study the electronic structure of PF_3 on several metal surfaces, including Pt(111), and concluded that the bonding was similar to that in PF_3 complexes.[24,25] A vibrational study of PF_3/Pt(111) using electron-energy-loss spectroscopy[21] observed the P–Pt stretch at 260 cm^{-1} in addition to the PF_3 bend and P–F stretch. The low resolution of EELS prevented observation of the band-shape variations which are the subject of this paper. Several ESDIAD (electron stimulated desorption ion angular distribution) studies[15–17] have addressed the issue of azimuthal order of adsorbed PF_3 and have investigated the barrier to rotation about the C_3 axis, a quantity for which the ESDIAD technique is uniquely capable of providing. All of the previous studies indicated that PF_3 bonds to on-top sites on metal surfaces via charge donation from the lowest occupied orbital of PF_3, the $8a_1$, with back donation from the metal into the lowest unoccupied orbital, the $7e$. Electronic structure calculations of PF_3 on Ni(111) (Ref. 26) support this basic bonding mechanism which is the same as for transition metal complexes of PF_3 (Refs. 24 and 25).

We previously[2,3] argued that the PF_3 ligand forms only terminal, rather than bridging, bonds to metal atoms in transition-metal complexes. However, very recent work has revealed the existence of triply coordinated PF_3 in complexes containing Pd_3 (Ref. 27) and Pt_3 (Ref. 28) triangles. Complexes containing such metal units serve as valuable analogues to transition-metal surfaces.[29] Although it is no longer possible to assert that multiple coordination is not a characteristic of PF_3 bonding to metals, the weight of the evidence still favors on-top site bonding on Pt(111).

In interpreting our data, we assume that the local bonding structure deduced in previous surface studies of chemisorbed PF_3 is correct. Our purpose here is to address the following issues which have not been dealt with previously. What is the origin of the strong coverage dependence of the P–F stretch frequency? Can dipole-dipole coupling and a simple island formation model quantitatively explain the behavior of the P–F stretch band shape? What are possible origins of the next-nearest-neighbor attractive interactions which must be present for island formation to occur? Can the two components of the P–F stretch be explained without invoking island formation? Why does the symmetric PF_3 bend remain as a single sharp band under the same conditions that lead to a splitting of the P–F stretch band? In addition to these questions, we present results on the deconvolution of the P–F stretch band components which allow us to quantify the relative numbers of molecules in the two phases on the surface. This data can then be directly compared with the sort of results obtainable through Monte Carlo simulations of the island formation process. Such a comparison offers the best hope of extracting from our infrared data a microscopic understanding of the local environment for PF_3. The general procedures established here can then be applied to other adsorbate/substrate systems.

EXPERIMENTAL

Our apparatus has been described in detail elsewhere.[30] In short, it consists of a stainless-steel UHV chamber with a current base pressure of 8×10^{-11} Torr (based on an ion gauge calibrated for N_2) coupled to a dedicated commercial Fourier transform infrared (FTIR) spectrometer (Cygnus 25, Mattson Instruments, purchased in 1984). The chamber is now equipped with commercial low-energy electron diffraction (LEED) optics (Perkin Elmer Physical Electronics Division C15-120). Differentially pumped viton *O*-ring sealed CsI windows let the *p*-polarized IR beam enter and exit the UHV chamber. We used two different IR detectors in these experiments. The P–F stretch band was measured primarily with a liquid-nitrogen-cooled MCT (mercury–cadmium–telluride) detector with a cutoff near 800 cm^{-1}, while the lower-frequency region was studied using a liquid-helium-cooled silicon bolometer. The use of the bolometer is described in previous publications.[3,31]

The crystal cleaning[2,32] and PF_3 purification[2] procedures have been described earlier. Briefly, high-temperature oxygen treatments were employed to remove impurities–usually carbon and phosphorus. Impurity concentrations were monitored with Auger electron spectroscopy. LEED was used to verify that the substrate was well ordered and to observe the $(\sqrt{3}\times\sqrt{3})R\,30°$ PF_3 overlayer pattern.

For the IR experiments, the freshly cleaned crystal was cooled to 81 K and exposed to PF_3. Immediately after the exposure, an IR spectrum was recorded at 81 K which was used to assign the coverage from the calibration curve (*de-*

scribed in the results section) and was never included in further analysis. An equilibrium overlayer structure was then achieved by annealing at 300 K and an IR spectrum was obtained at 300 K. Then a series of spectra were recorded at 81, 160, and at 200 K in random sequence before recording the final spectrum again at 300 K. The purpose of recording spectra at 300 K before and after recording all other spectra was to check the effect of background adsorption during the experiment and to verify that temperature-dependent effects were reversible. The two spectra at 300 K agreed very well in nearly all cases. The variation in the intensities (the combined intensity of the two bands in the P–F stretch region) of these two spectra was always within 5% and mostly less than 2%. The two 81 K spectra, before and after annealing, differ markedly in the shape of the doublet demonstrating that adsorption at 81 K does not yield an equilibrium overlayer structure.

In the temperature-dependent studies where many spectra were recorded after exposure and between the two 300 K spectra, only 128 or 64 scans (64 and 32 seconds, respectively, of signal averaging) were collected. The instrumental resolution was increased to 0.5 cm^{-1} when the full width at half maximum (FWHM) was investigated near saturation coverage since the bandwidths were close to 2 cm^{-1} or less.

The two overlapping bands in the P–F stretch region were deconvoluted by fitting the observed line shapes with the sum of two Lorentzian functions by using the user-defined curve fitting option of the ASYSTANT software package (Asyst Technologies, Inc.) The Gauss–Newton algorithm was employed for the fitting process. The goodness of fit was judged from the value of the square of the multiple correlation function which was always about 0.99 or better. The multiple correlation function is defined as

$$R = (1 - \mathrm{Err}^2/\mathrm{Res}^2)^{1/2},$$

where

$$\mathrm{Err}^2 = \sum_{i=1}^{n} |y_i - F(x_i)|^2 \quad \text{and} \quad \mathrm{Res}^2 = \sum_{i=1}^{n} |y_i|^2.$$

In these equations the y_i's are the experimental data points of the absorptance spectrum and $F(x)$ is the fit function, i.e.,

$$F(x) = a/[(x - x_{10})^2 + f_1^2] + b/[(x - x_{20})^2 + f_2^2].$$

The full width at half maxima of the two Lorentzians are then taken as $2f_1$ and $2f_2$, while the areas are given by $\pi a/f_1$ and $\pi b/f_2$. The x_{10} and x_{20} represent the frequencies of the maxima of the Lorentzians. A visual inspection of the fitted curves showed that the Lorentzian fit was always relatively better for the component of the doublet which had greater intensity than the weaker one. Fits using Gaussian lineshape functions were always inferior to fits using Lorentzian functions.

RESULTS

In order to provide a detailed microscopic interpretation of our data, the establishment of absolute PF_3 coverages was essential. Relative coverages were determined from thermal desorption peak areas. A series of thermal desorption spectra as a function of increasing exposure are shown in Fig. 1. These results were obtained by exposing the surface at 81 K while our earlier thermal desorption results[2] were obtained after 300 K exposures. Absolute coverages were then assigned by taking the area of the saturation coverage at 300 K which was assigned a coverage of 0.33 ML based on observation of the $(\sqrt{3}\times\sqrt{3})R$ 30° LEED pattern. Each thermal desorption measurement was preceded by an infrared spectrum of the P–F stretch region. In this way the relationship between the IR peak area and coverage was established so that IR areas obtained in subsequent experiments could be used as a measure of coverage. This method was found to be more reliable than attempting to assign coverages from calibrated PF_3 exposures. The relationship between IR peak area and coverage is shown in the inset of Fig. 1.

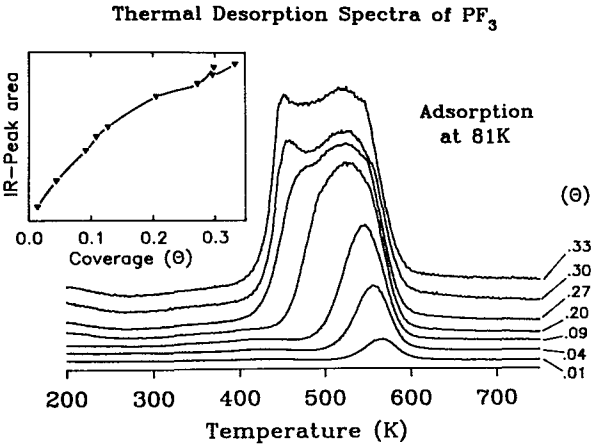

FIG. 1. Thermal desorption spectra as a function of coverage after exposure at 81 K. The absolute coverage is based on a saturation coverage of 0.33 monolayer and relative coverages on the thermal desorption peak areas. The inset shows the integrated IR peak areas for the P–F stretch as a function of coverage.

As noted in the Introduction, we have reported the changes in the P–F stretch as a function of exposure and the frequency and FWHM of the PF_3 symmetric bend at saturation coverage in earlier publications. In this paper we present coverage and temperature dependence of the PF_3 symmetric bend. The variations in the frequency and FWHM of this band with increasing PF_3 exposure at 81 K are shown in Fig. 2. For the PF_3 bend it was not possible to obtain accurate

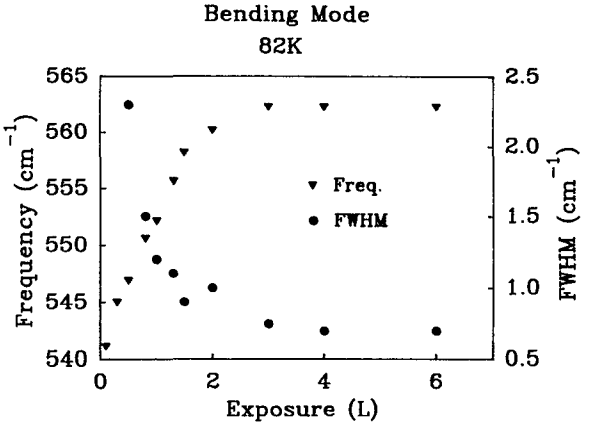

FIG. 2. The dependence of the frequency and FWHM on coverage for the PF_3 symmetric bend.

values for the coverage nor was it particularly important. The FWHM decreases from 2.3 cm^{-1} at the lowest coverage to 0.7 cm^{-1} at saturation coverage while the frequency increases from 541 to 562 cm^{-1}. Both changes are small compared with the P–F stretch which shows a total coverage dependent shift of 50 cm^{-1} and undergoes changes in FWHM of more than a factor of 10 from the narrowest to the broadest lines. Furthermore, the δPF_3 band does not split into two components at intermediate coverages as does the P–F stretch band. It is thus evident that the PF_3 bend is far less sensitive to adsorbate–adsorbate interactions than is the P–F stretch.

The contrast between the two modes is further illustrated by the temperature dependence at constant coverage shown in Fig. 3. The spectra at each temperature were obtained simultaneously for both modes although for clarity only the spectral region around each band is shown. From the shape of the doublet in the stretch region we estimated the coverage to be about 0.20 ML. The Si bolometer was used at resolutions of 0.5 and 0.25 cm^{-1} with a low pass filter having a nominal cutoff at 800 cm^{-1} combined with a relatively high interferometer mirror speed leading to a loss of detector response above 630 cm^{-1}. These conditions improve the signal-to-noise ratio (SNR) in the region of the umbrella mode at the expense of the SNR in the P–F stretch region. The top spectrum was obtained immediately after exposure at 300 K, while the bottom 300 K spectrum was obtained after acquiring the 150 K and 82 K spectra. Whereas the P–F stretch shows splitting into two components

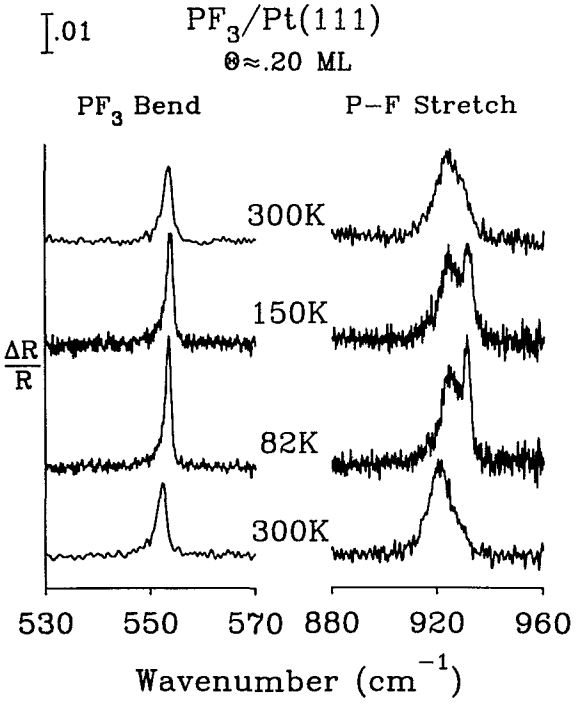

FIG. 3. Band-shape dependence of the P–F symmetric stretch and PF_3 symmetric bend on temperature at a coverage of 0.2 ML. This coverage was estimated based on the shape of the P–F stretch doublet. A resolution of 0.5 cm^{-1} was used for the 300 K spectra; it was increased to 0.25 cm^{-1} for the 82 and 150 K spectra.

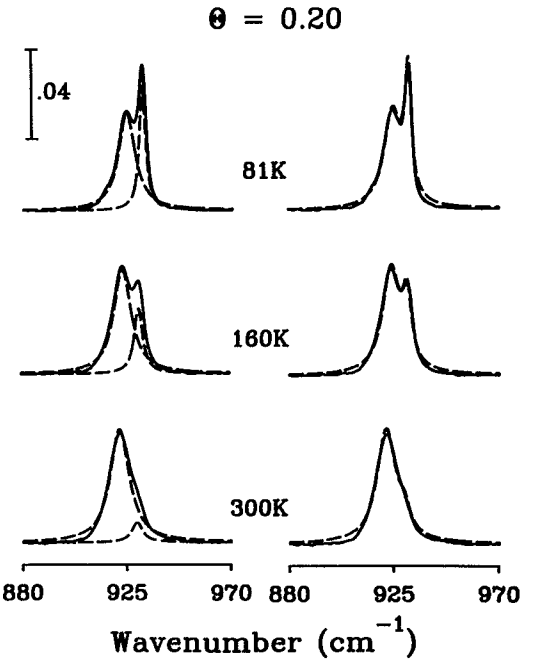

FIG. 4. Fits of the experimental (solid curve) band shape of the P–F stretch to the sum of two Lorentzian functions. The dashed curves represent the separate Lorentzians on the left and their sum on the right.

upon cooling, the PF_3 bend becomes sharper and slightly asymmetric with tailing to lower frequencies. Again it is evident that the symmetric PF_3 bend is relatively insensitive to the changes in the overlayer structure which strongly affect the P–F stretch. For these reasons our detailed analysis, the purpose of which is to learn more about the overlayer structure, is confined to the P–F stretch band.

To obtain additional information about the two types of environment assumed to be responsible for the two components of the P–F stretch, it is desirable to deconvolute the two components of the P–F stretch band. Figure 4 shows some experimental line shapes fitted with the sum of two Lorentzian functions. It is seen that the overall band shape is fitted well by only two distinct peaks indicating that all of the molecules clearly belong to one of two distinct types.

The individual intensities, full widths at half maxima, and the frequencies of the two deconvoluted bands as a function of coverage at four different temperatures are given in Figs. 5–7. Qualitatively, the plots are similar at all four temperatures. These plots reveal several characteristics of the coverage and temperature dependence for the two components.

In Fig. 5 we see that the low-frequency band goes through a maximum intensity and that this maximum shifts towards higher coverage with increasing temperature, from 0.15 ML at 81 K to 0.20 ML at 300 K. The rise and fall in intensity of this band is roughly linear. The high frequency component is first observed at about $\theta = 0.10$ ML indicating that ordered patches of PF_3 in the $(\sqrt{3}\times\sqrt{3})R\,30°$ structure begin to form at this coverage. Although this component is first observed at 0.10 ML, it does not increase in intensity until a coverage of $\theta = 0.15$–0.20, depending on the temperature, is reached at which point the intensity of the low-

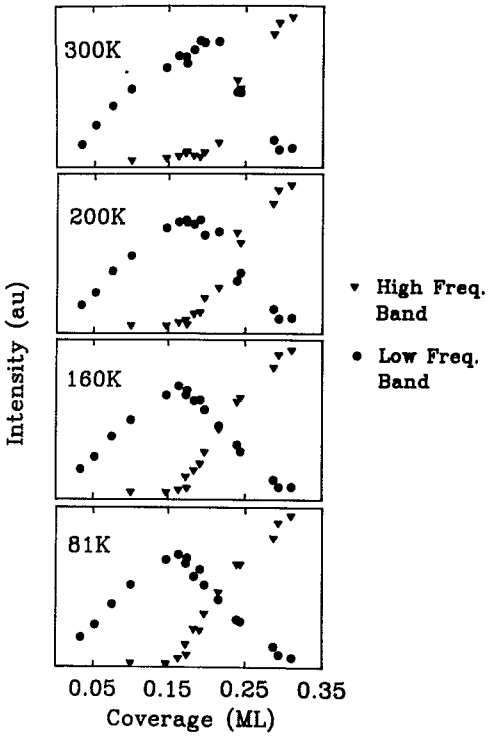

FIG. 5. The intensities of the deconvoluted components of the P–F stretch as a function of coverage at the indicated temperatures.

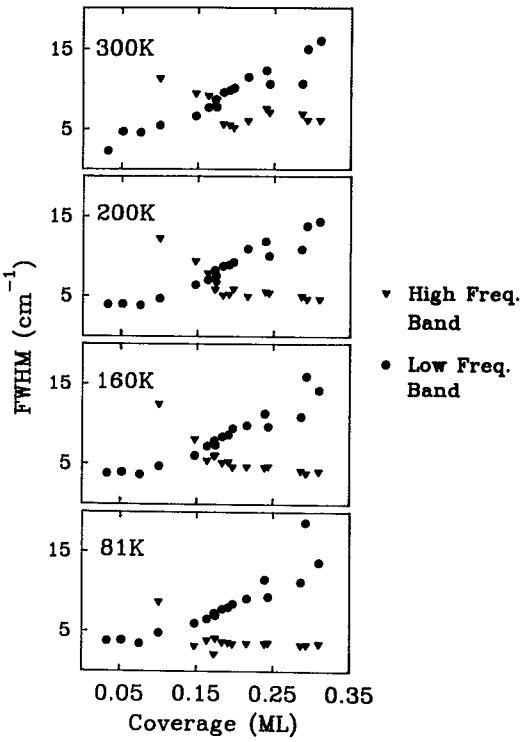

FIG. 7. The full widths at half maximum (FWHM) of the deconvoluted components of the P–F stretch as a function of coverage at the indicated temperatures.

frequency band begins to decrease. Beyond $\theta = 0.20$ ML, the high-frequency band dominates the spectrum.

Figure 6 indicates that the high-frequency component first appears around 925 cm^{-1}, nearly 10–13 cm^{-1} higher than the low-frequency band, the exact difference depending somewhat on temperature. This value of 925 cm^{-1} which we associate with molecules in islands with the $(\sqrt{3}\times\sqrt{3})R$ 30° structure represents only half of the total shift from 900 to 950 cm^{-1} associated with the formation of a complete $(\sqrt{3}\times\sqrt{3})R$ 30° overlayer. At 300 K, the frequency of the high-frequency band appears to increase continuously with coverage. However, at lower temperatures it remains nearly constant in the coverage region $\theta = 0.10$–0.20 ML. For $\theta \geqslant 0.2$ ML its frequency increases until saturation while the low-frequency band acquires a constant position invariant with temperature. A comparison of Figs. 5 and 6 shows that the low-frequency band acquires a constant frequency at a coverage higher than when its intensity reaches maximum, so that there is a small coverage range in which its frequency is still increasing despite its decreasing intensity.

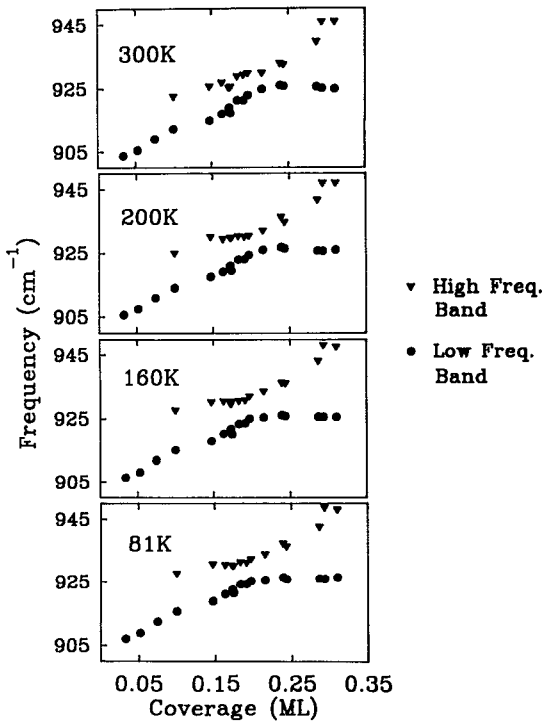

FIG. 6. The frequencies of the deconvoluted components of the P–F stretch as a function of coverage at the indicated temperatures.

The slopes of the increasing frequency with coverage plots of Fig. 6 seem to be the same for the two bands, i.e., the slope of the low-frequency band in the region $\theta = 0$–0.20 ML is nearly same as that of the high-frequency band at coverages greater than 0.25 ML. It appears to indicate the presence, at all coverages, of some overall long-ranged interaction and that the high-frequency band is simply shifted upwards by an additional effect which is present only in the dense clusters.

Figure 7 shows the dependence of the FWHM of the two components of the P–F stretch as a function of coverage. At the lowest coverages the FWHM of the low-frequency band is constant with coverage until the high-frequency component appears. The FWHM of the high-frequency component shows an initial decrease and then reaches a constant final value at a coverage of about 0.15 ML at which point the

FWHM of the low-frequency component begins to increase. It is interesting to note that the FWHM of the high-frequency component at high coverage has roughly the same value as the low-frequency component at low coverages. Note that the increase with coverage in the FWHM of the low-frequency component coincides with the decrease in its intensity but that its frequency is still increasing at that coverage. The increasing width of the low-frequency band after $\theta = 0.10$ suggests a widening distribution of environments for the molecules in the lower density phase.

An important issue in our analysis is whether the ratio of relative intensities of the two components of the P–F stretch is equal to the ratio of the number of molecules in the two environments. In general, there is no reason to expect a linear relationship between IR intensity and coverage and there is no reason to expect the IR cross section for PF_3 molecules in the two environments to be equal. In many adsorbate systems screening of the dynamic dipole moments by the electronic polarizability of the molecules leads to a nonlinear relationship between IR intensity and coverage[12] and in some cases the maximum intensity does not occur at maximum coverage.[7] The nonlinearity of the total P–F stretch intensity as a function of coverage as displayed in the inset of Fig. 1 is typical. In addition to this screening effect, dipole–dipole coupling leads to an enhancement of the intensity of higher-frequency bands relative to lower-frequency bands. This latter intensity transfer is generally a larger effect than that due to screening. Therefore, it would not be surprising to find that the effective IR cross section for the molecules in the higher density phase (giving rise to the high-frequency band) to be different from molecules in the lower density phase (leading to the low-frequency band). However, this does not appear to be the case. This is demonstrated by examining the total IR area at constant coverage as a function of temperature for the spectra in Fig. 8. The drastic change in the shape of the P–F stretch doublet is most obvious, although the intensity of the low-frequency band is still slightly greater than that of the high-frequency band at this coverage. Similar results at slightly higher coverages show a reversal in the relative intensity of the two components. The separate deconvoluted intensities of the two components and their sum is shown in Fig. 9 as a function of temperature. It is seen that the separate intensities are strongly temperature dependent but that the sum is not. This proves that the cross sections for the two types of molecules are approximately the same. This is further demonstrated by the plot of the intensity of the low-frequency band as a function of the intensity of the high-frequency band. The plot shows a linear relationship with a slope of one indicating a simple exchange of molecules from one environment to the other. Thus it is valid to take the relative intensity of the two IR components as a measure of the relative numbers of the two types of molecules.

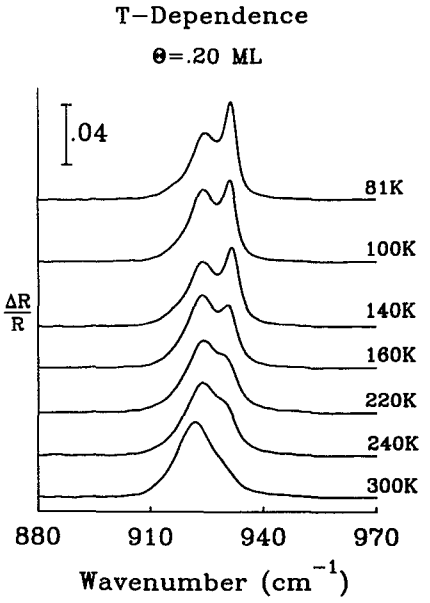

FIG. 8. Temperature dependence of the P–F stretch at a coverage of 0.2 ML. The spectra were recorded in a random sequence.

DISCUSSION

The central fact of our study is the strong positive shift in the P–F stretch frequency with increasing PF_3 coverage. It is this fact which leads us to conclude that the higher-frequency component of the split P–F stretch band is associated with PF_3 molecules in islands and the lower-frequency component to PF_3 molecules in a lower density phase. It is therefore important to consider in detail the source of the frequency shift with coverage. Such shifts are usually divided into two types. Coupling shifts are a consequence of the identical frequencies of the individual mole-

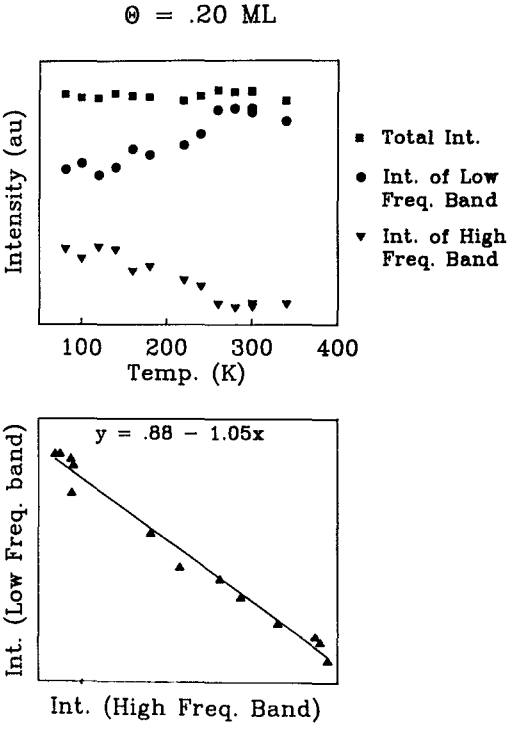

FIG. 9. Intensity dependence of the two deconvoluted components of the P–F stretch on temperature. The upper panel shows that while the separate intensities display a strong dependence on temperature their sum does not. The lower panel shows that there is a 1:1 exchange of molecules between the two environments.

cules. The most important coupling mechanism is the dipole–dipole interaction. Chemical or static shifts are a consequence of changes in the intramolecular bonding. The two types of shifts can be experimentally separated through isotopic dilution experiments. Unfortunately such experiments are not possible for PF_3 as only a single stable isotope exists for both phosphorous and fluorine. Nevertheless, we can discuss how chemical and dipole–dipole coupling shifts pertain to this system. We start by considering dipole–dipole coupling.

The frequency, ω, due to dipole–dipole coupling relative to the adsorbate frequency in the limit of zero coverage, ω_0, is given by[33]

$$(\omega/\omega_0)^2 = 1 + \alpha_v U/(1 + \alpha_e U), \quad (1)$$

where α_v and α_e are the vibrational and electronic polarizabilities, respectively, of the adsorbate and U is the dipole sum including contributions from image dipoles. The coverage dependence is contained in U which depends solely on the lattice and is independent of the properties of the adsorbate. The inclusion of α_e takes into account the screening of the dipoles due to the electronic polarizability of the adsorbate. In the above expression ω_0 is the singleton frequency and includes the self-image shift.

To estimate the size of the dipole coupling shift we need values for α_v and α_e for chemisorbed PF_3. The value of U for the $(\sqrt{3}\times\sqrt{3})R$ 30° lattice on Pt(111) using a dipole-image plane distance of 1.1 Å is 0.16 $Å^{-3}$. For the frequency in the limit of zero coverage, we use $\omega_0 = 901$ cm^{-1}. We obtain a value for α_v of 0.56 $Å^3$ from measurements of the absolute intensity of the P–F symmetric stretch for gas phase PF_3 (Ref. 34) (the details are given in the Appendix). Based on values of similar molecules, we estimate α_e to be about 5 $Å^3$ for PF_3. Apparently α_e for gas phase PF_3 has not been measured. These numbers yield a dipole–dipole coupling shift of 22 cm^{-1} compared to the total shift with coverage of 50 cm^{-1}. Thus either the parameters used are not valid for chemisorbed PF_3 or the shift is not due to dipole–dipole coupling alone. We can obtain a total shift of 50 cm^{-1} from Eq. (1) if we let $\alpha_v = 1.27$ $Å^3$ while leaving all other parameters the same. Note that an even larger increase is observed for CO where α_v increases from 0.057 $Å^3$ in the gas phase to 0.22 $Å^3$ for CO chemisorbed on Pt(111).[35] Similarly, a value of $\alpha_v = 0.93$ $Å^3$ for the symmetric bend is needed to obtain the observed shift of 21 cm^{-1} rather than the value of 0.41 $Å^3$ for gas phase PF_3. Although it is plausible that the α_v's for PF_3 increase substantially upon chemisorption, there are other factors which suggest that the shifts with coverage can not be attributed solely to dipole–dipole coupling alone.

An inherent problem in dipole–dipole coupling theory is the precise knowledge of the dipole sum for partially filled overlayers. The basic parameter governing the dipole sum is the distribution of intermolecular distances which, in turn, depends on adsorbate–adsorbate interactions. Therefore, the dipole sum and, hence, the nature of the frequency shift with coverage, as given by Eq. (1), is largely dependent on the adsorbate–adsorbate interactions. Abrupt changes in the adsorbate–adsorbate distance can lead to a sudden change in the dipole sum. As discussed by Mahan and Lucas[33] for a random growth of the overlayer, the dipole sum varies as θ, while if the adsorbate species tend to maintain constant uniform separation, the dipole sum goes as $\theta^{3/2}$. Both these situations lead to a rather smooth variation of frequency with coverage. There is certainly no possibility for a second band at any coverage. Physically, the first situation can arise when interadsorbate interactions are very weak, while the latter situation is likely when adsorbate–adsorbate interactions are strongly repulsive and long range, for example, as in alkali metal overlayers on metals.[36] In fact, each adsorbate-substrate system presents a unique case in terms of the exact distribution of intermolecular distances and hence, for evaluation of the dipole sum.

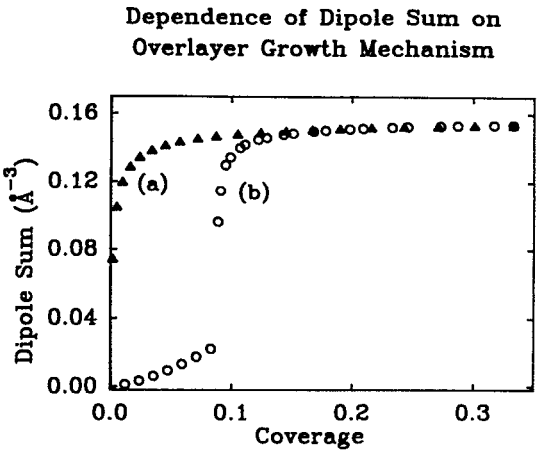

FIG. 10. The dependence of the dipole sum on the mechanism of the overlayer growth. A hexagonal lattice with 20 consecutive rings around a central molecule (1260 molecules total) is assumed to represent an infinite overlayer. (a) Successive rings of molecules are placed around the central molecules. (b) First, coverage was increased by maintaining constant uniform intermolecular separation until a $(2\sqrt{3}\times 2\sqrt{3})R$ 30° structure was formed. Then molecules were placed in successive hexagonal rings around the central molecule to fill the vacant sites, forming a $(\sqrt{3}\times\sqrt{3})R$ 30° structure.

Figure 10 shows the variation of the dipole sum based on the two models of overlayer growth. The first case, Fig. 10(a), would result when attractive interactions alone are present. The second case, Fig. 10(b), would apply when additional long-range repulsive interactions are also present. When attractive interactions dominate, clustering is the likely result and the local coverage quickly reaches the saturation coverage. For reasons of ease of calculation and due to similarity with the present system, a $\sqrt{3}$ structure is assumed for the clusters and the molecules are added in successive hexagonal rings around a central reference molecule. The figure shows that the first hexagonal ring of molecules accounts for about 50% of the value of the sum obtained for infinitely large islands. Thus, for molecules in even moderately large islands, the P–F stretch frequency would be essentially the same as the frequency at saturation coverage. Furthermore, at coverages where the two components of the P–F stretch are of comparable intensity, the higher-frequency component occurs near 932 cm^{-1}, a shift from the zero-coverage limit of only about 60% of the total shift with coverage. Figure 10 implies that islands for which the P–F

stretch is 932 cm^{-1} must be quite small with at most two hexagonal rings, or only 19 molecules. We see from Fig. 6 that for a coverage of 0.2, the intensity of the two components is about equal. If the number of molecules in islands of local coverage of 0.33 is equal to the number in the lower density phase and the total coverage is 0.2, then the density in the second phase would be only 0.08 ML. At a total coverage of 0.08 there is only one component to the P–F stretch and it has a frequency of only 910 cm^{-1}, considerably less than the 925 cm^{-1} observed for the low-frequency component at a total coverage of 0.2. This higher frequency might be explained by coupling between molecules in the two phases.

In the second case the overlayer growth at lower coverages is expected to be dictated by the repulsive interactions which tend to maintain a constant uniform separation between the adsorbate molecules. As an example, we assumed that the minimum uniform constant adsorbate–adsorbate distance which is possible in the presence of the repulsive interactions is twice that of the saturation coverage, which we again choose as $\sqrt{3}a$, for consistency. Hence, the dipole sum should increase as $\theta^{3/2}$ (Ref. 33) until a $(2\sqrt{3}\times 2\sqrt{3})R$ 30° structure is formed on the surface. The additional molecules have to then occupy the vacant sites between the existing molecules to form the final $\sqrt{3}$ structure. These molecules are added around a central reference molecule in successive rings at $\sqrt{3}$ separation, so that all vacancies are filled and a $\sqrt{3}$ structure results. Now, however, the dipole sum does not increase with coverage in a smooth manner, instead there is a jump near $\theta = 0.08$, when the intermolecular distances are abruptly reduced. This can clearly lead to an additional high frequency band after $\theta = 0.08$. Another consequence of the abrupt reduction in intermolecular distances leading to the formation of a $\sqrt{3}$ domain will be an increased electrostatic field around the molecules than in the less dense disordered domain. As Efrima and Metiu[37,38] have shown, the increased electrostatic field in the islands can lead to an upward frequency shift and thus, be responsible for the high-frequency band. It is tempting to suggest that this second overlayer growth mechanism applies to the PF_3/Pt(111) system, since the high-frequency band is initially observed at $\theta = 0.10$. However, it is difficult to explain the strong temperature dependence by this model. Also no other ordered structure besides the $\sqrt{3}$ structure has ever been observed.

The most compelling evidence that dipole–dipole coupling alone is not responsible for the coverage dependence of the P–F stretch is the absence of a two-component structure for the umbrella mode under conditions where two components are observed for the P–F stretch. In Fig. 3 the high-frequency component of the P–F stretch is at 932 cm^{-1}, or about half of the total shift for this mode. The separation between the two components of the P–F stretch is ≈ 7 cm^{-1} at this coverage. The dipole-coupling model would imply that the umbrella mode should display two components with a separation equal to the same fraction of the total shift with coverage. Thus we would have expected to observe two components of the umbrella mode separated by $(7/50)21 = 3$ cm^{-1}, a separation which would be easily observable. Instead we observe a single, although asymmetric, band with a FWHM of 2 cm^{-1}. The sensitivity of the P–F stretch band to adsorbate interactions to which the PF_3 bend is relatively insensitive seems incompatible with the dipole–dipole coupling shift described by Eq. (1). Similar arguments also rule out the vibrational coupling through metal electrons[39] as the sole interaction.

The different behavior of the two bands does provide some insight as to the origin of the sensitivity of the P–F stretch towards the intermolecular interactions. The results of Fig. 3 suggest that local chemical effects are responsible for the two components of the P–F stretch rather than different degrees of dipolar coupling. This is supported by an EELS study[22] of PF_3 and NH_3 coadsorption on Ru(001). It was observed that the P–F stretch frequency shifts downwards by 60–90 cm^{-1} in the presence of coadsorbed NH_3 while no change in frequency was observed for the PF_3 bend. This result indicates the local interactions to which the P–F stretch is so sensitive are chemical in nature. In considering the origin of this effect, it should be kept in mind that the normal modes of A_1 symmetry for gas phase PF_3 have appreciable amounts of both bond-stretching and bond-bending character with the higher-frequency mode having more contribution from the stretch symmetry coordinate and the lower-frequency mode having slightly more contribution from the angle changing symmetry coordinate.[34] Thus, the actual atomic motions associated with the two modes are not as different as might be presumed.

The origin of chemical shifts for PF_3 and CO should be quite similar given the similarity in bonding properties.[24–29] The bonding of both molecules to metals involves donation of charge from the highest occupied orbital (HOMO) and back donation into the lowest unoccupied orbital (LUMO) of the adsorbate. The HOMO of PF_3 is the $8a_1$ orbital which is mainly a phosphorus lone pair with some P–F antibonding character. The LUMO is a $7e$ orbital which is also antibonding with respect to the P–F bond. Thus, factors which increase σ donation should increase the frequency of the P–F stretch while increased back donation into the $7e$ orbital should decrease its frequency. Because the bonding of PF_3 to metals is known to involve both σ donation and π backbonding, the closeness of the P–F stretch frequency of gas phase PF_3 to PF_3 at low coverages on Pt(111) and in $Pt(PF_3)_4$ indicates a near cancellation of an upward shift due to σ donation and a downward shift due to π backbonding. A positive chemical shift would then imply a decreasing amount of π backbonding with increasing coverage. Ueba[40] has developed a compelling correlation between the sign of chemical shifts and work-function changes for chemisorbed CO which we successfully used to explain the large negative chemical shift we observed for N_2 on Ni(110).[41] To apply this model to the present case it would be best to know the coverage dependence of the work function. However, this has not yet been measured although the net change upon saturation has been determined to be -0.5 eV.[14] This indicates that at a saturation coverage of 0.33 ML PF_3 is a net electron donor. Reduced backdonation (and hence a positive chemical shift) would be expected if the $7e$ energy level increases in energy with coverage which would be expected if PF_3 is a net acceptor. This would be the conclusion if the

work function change is positive upon PF_3 adsorption (as it is on all of the other metals[14]) at low coverage and only became negative at higher coverages. However, the work function change due to CO adsorption on Pt(111) is negative, as it is on the noble metals, and so is the chemical shift. If PF_3 were to behave similarly and also have a negative chemical shift, then the dipole–dipole coupling shift would be even larger than the observed 50 cm^{-1}. This would then imply an even greater discrepancy between the values of the vibrational polarizability of gas-phase PF_3 and chemisorbed PF_3 than necessary to account for a 50 cm^{-1} shift. It is instructive to point out that the two molecules differ in their desorption behavior[18] in the presence of the electron donor coadsorbate potassium, which is expected to increase the π backdonation.

Given the large total positive shift with increasing coverage it is at least plausible that a positive chemical shift is present in addition to dipole coupling. Whereas, dipole coupling should be fairly long range, a chemical shift is likely to be short range. We thus speculate that island molecules have a higher frequency because they are close enough to other molecules to experience a short-ranged positive chemical shift. The combination of a positive chemical shift with the dipole coupling shift would then result in the net 50 cm^{-1} shift observed with coverage. The shape of the frequency versus coverage plots for the two components in Fig. 6 is indeed suggestive of an overall linear increase in frequency with coverage to which is added a positive shift for some molecules at a coverage of 0.1 ML.

The presence of PF_3 islands on Pt(111) implies an attractive lateral interaction. The attraction may be a direct intermolecular interaction or be an indirect metal-mediated interaction. The possible direct interactions can be of several types. The large permanent dipole moment of 1.0 D for gas phase PF_3 implies a long-range dipole–dipole repulsive interaction varying as R^{-3}. Similarly, quadrupole–quadrupole, octapole–octapole, etc., interactions will also be repulsive. However, the induced dipole-induced dipole (dispersion) interaction is attractive and short range with a R^{-6} dependence. For CO physisorbed on NaCl surfaces, Disselkamp *et al.*,[42] have listed values for the various types of adsorbate–adsorbate interactions based on parameters for gas phase CO. The dispersion interaction is the largest and tentatively suggests a net attraction between the molecules. However, even for CO many of the needed parameters are not known to a high enough accuracy to definitively conclude that the net interaction is attractive. Far less data is available for gas phase PF_3 and even if it were it is not known how much the values would change for the chemisorbed molecule. While the dipole–dipole repulsion will be large, the polarizability is also large which would favor an attractive interaction. Thus simple qualitative arguments can not be used to decide if the direct interaction should be attractive or repulsive at the distances present in the $(\sqrt{3}\times\sqrt{3})R\,30°$ structure. However, given the different ranges of the interactions, it is reasonable to assume that at large distances the interaction is repulsive and that it may become attractive at shorter distances. There is certainly nothing in our data that contradicts this.

In addition to the direct through-space interactions, indirect through-metal interactions have been well documented through electronic structure calculations.[43–52] An atom or molecule chemisorbed at one metal site can perturb the electronic structure at neighboring sites to make these sites either more or less energetically favored relative to unperturbed sites. Such metal mediated interactions can lead to an effective adsorbate–adsorbate interaction which is either attractive or repulsive. In fact, the sign of the interaction can alternate with distance from the adsorbate. The presence of such oscillatory interactions has been used to explain the multitude of ordered overlayer structures seen for a given adsorbate/metal system. The interaction is fairly local and extends only a few lattice constants away from an adsorbate site. There are numerous examples that indicate such metal-mediated interactions can overcome direct Coulombic repulsions between adsorbates to give rise to a net pair-wise attractive interaction. Thus both the direct induced dipole-induced dipole interaction or a metal-mediated interaction can plausibly explain the presence of an attractive interaction between the PF_3 molecules despite the obvious repulsive interaction between large and parallel permanent dipole moments.

While it may not be possible to identify the physical origin of the intermolecular interactions manifested in the temperature and coverage dependence of the infrared spectrum for the PF_3/Pt(111) system, it may be possible to quantify the interaction. For assumed values of the interaction potential, one can carry out simulations of the adsorbate structure using Monte Carlo methods. This is a standard approach[1] often used to simulate surface and adsorbate phase transitions as observed with LEED. Such simulations have recently been used to gain a better understanding of the adsorbate structures assumed by CO on Pt(111),[53] which have been characterized experimentally with both LEED and IRAS. Our results indicate that the adsorbate structures assumed by PF_3 on Pt(111) should also be amenable to such an approach.

CONCLUSIONS

Our results for the PF_3 symmetric bend and P–F symmetric stretch fundamentals of PF_3 chemisorbed on Pt(111) reveal that adsorbate–adsorbate interactions can have dramatically different effects on different intramolecular vibrational modes of polyatomic adsorbates. This difference along with other considerations suggest that dipole–dipole coupling alone can not account for the two-component structure of the P–F stretch band. Instead a short-range chemical shift which preferentially affects the P–F stretch vibration is likely involved in addition to the longer-range dipole–dipole coupling interaction. Although simple quantitative models exist which can relate the size and even shape of two-dimensional adsorbate clusters to observed vibrational frequencies in the case of dipole–dipole coupling, no such quantitative models exist for chemically induced frequency shifts. Thus the direct extraction of information on the structure of PF_3 islands and the disordered PF_3 phase on this surface is not presently possible. However, the data pre-

sented here should be suitable for direct quantitative comparison with results from a Monte Carlo simulation.

APPENDIX

Although a variety of expressions exits for the absolute intensities of vibrational transitions, they can all be related to the vibrational polarizability. Here we describe the relations we used to obtain vibrational polarizabilities from the integrated intensities. Persson and Ryberg[53] relate the vibrational polarizability, α_v, to the matrix element of the dipole moment operator $\langle a|\mu|b\rangle$ with

$$\alpha_v = (2/\hbar\nu)|\langle a|\mu|b\rangle|^2.$$

Levin and Adams[34] report experimental values for the integrated intensities of the symmetric P–F stretch of $\Gamma_1 = 12.36$ cm^2/mM and for the symmetric PF_3 bend of $\Gamma_2 = 4.957$ cm^2/mM, where mM is milli-molar. Their quantity Γ is defined by

$$\Gamma = (RT/pl)\int \ln(I_0/I)d\ln\nu,$$

where p is the pressure of the gas in centimeters of mercury, R is the gas constant in liter-centimeters per mole degree, T the temperature, and l is the cell path in centimeters. From the Beers law equation

$$I/I_0 = \exp(-k_\nu l),$$

we obtain

$$\Gamma = (RT/p)\int k_\nu d\ln\nu = (RT/p)\int (k_\nu/\nu)d\nu$$

$$\approx (RT/p\nu_0)\int k_\nu\, d\nu,$$

where the approximation simply involves replacing the wave number, ν, in the integrand with its value, ν_0, at the band center since ν does not vary significantly over the band. The relationship between the absorption coefficient, k_ν, in units of cm^{-1} is related to other measures of the transition strength such as the Einstein B coefficient, the absorption cross section, σ, and the dipole operator matrix element.[54] From such relationships one obtains

$$\alpha_v = 3\Gamma/(4\pi^3\omega N_0),$$

where Γ is, as before, in cm^2/mM, $N_0 = 6.022\times10^{20}$ (mM)$^{-1}$ is Avogadro's number expressed in molecules per mM, and ω is the wave number of the vibrational band in cm^{-1}. This expression yields α_v in units of cm^3. In this way we obtain the values of $\alpha_v = 0.56$ and 0.41 Å^3 for the symmetric stretch and bend, respectively, from the absolute intensity data[34] for gas phase PF_3.

[1] L. D. Roelofs and P. J. Estrup, Surf. Sci. **125**, 51 (1983).
[2] S. Liang and M. Trenary, J. Chem. Phys. **89**, 3323 (1988).
[3] V. K. Agrawal and M. Trenary, J. Vac. Sci. Technol. A **7**, 2235 (1989).
[4] G. Michalk, W. Moritz, H. Pfnür, and D. Menzel, Surf. Sci. **129**, 92 (1983).
[5] H. Pfnür and H. J. Heier, Ber. Bunsenges. Phys. Chem. **90**, 272 (1986).
[6] E. D. Williams, W. H. Weinberg, and A. C. Sobrero, J. Chem. Phys. **76**, 1152 (1982).
[7] H. Pfnür, D. Menzel, F. M. Hoffmann, A. Ortega, and A. M. Bradshaw, Surf. Sci. **93**, 431 (1980).
[8] H. Pfnür, P. Feulner, H. A. Engelhardt, and D. Menzel, Chem. Phys. Lett. **59**, 481 (1978).
[9] M. Golze, M. Grunze, and W. Hirschwald, Vacuum **31**, 697 (1981).
[10] J. W. Niemantsverdriet, K. Markert, and K. Wandelt, Appl. Surf. Sci. **31**, 211 (1988).
[11] F. M. Hoffmann, Surf. Sci. Rep. **3**, 107 (1983).
[12] P. Hollins and J. Pritchard, Prog. Surf. Sci. **19**, 275 (1985); P. Hollins, Surf. Sci. **107**, 75 (1981).
[13] R. Ryberg, Phys. Rev. B **40**, 865 (1989).
[14] F. Nitschke, G. Ertl, and J. Küppers, J. Chem. Phys. **74**, 5911 (1981).
[15] M. D. Alvey, J. T. Yates, and K. J. Uram, J. Chem. Phys. **87**, 7221 (1987).
[16] M. D. Alvey and J. T. Yates, Jr., J. Am. Chem. Soc. **110**, 1782 (1988).
[17] A. L. Johnson, S. A. Joyce, and T. E. Madey, Phys. Rev. Lett. **61**, 2578 (1988).
[18] E. L. Garfunkel, J. J. Maj, J. C. Frost, M. M. Farias, and G. A. Somorjai, J. Phys. Chem. **87**, 3629 (1983).
[19] K. L. Shanahan and E. L. Muetterties, J. Phys. Chem. **88**, 1996 (1984).
[20] G. Blyholder and R. Sheets, J. Colloid Interf. Sci. **46**, 380 (1974).
[21] Y. Zhou, G. E. Mitchell, M. A. Henderson, and J. M. White, Surf. Sci. **214**, 209 (1989).
[22] Y. Zhou, Z.-M. Liu, and J. M. White, Surf. Sci. **230**, 85 (1990).
[23] X. Guo, J. T. Yates, Jr., V. K. Agrawal, and M. Trenary, J. Chem. Phys. **94**, 6256 (1991).
[24] Th. Kruck, Angew. Chem. Int. Edit. **6**, 53 (1967).
[25] J. F. Nixon, Adv. Inorg. Chem. **29**, 41 (1985).
[26] A. W. E. Chan and R. Hoffmann, J. Chem. Phys. **92**, 699 (1990).
[27] A. L. Balch, B. J. Davis, and M. M. Olmstead, J. Am. Chem. Soc. **112**, 8592 (1990).
[28] A. M. Bradford, G. Douglas, L. Manojlovic-Muir, K. W. Muir, and R. J. Puddephatt, Organometallics **9**, 409 (1990).
[29] R. J. Puddephatt, L. L. Manojlovic-Muir, and K. W. Muir, Polyhedron **9**, 2767 (1990).
[30] M. E. Brubaker and M. Trenary, J. Chem. Phys. **85**, 6100 (1986).
[31] I. J. Malik and M. Trenary, Surf. Sci. **214**, L237 (1989).
[32] I. J. Malik, M. E. Brubaker, S. B. Mohsin, and M. Trenary, J. Chem. Phys. **87**, 5554 (1987).
[33] G. D. Mahan and A. A. Lucas, J. Chem. Phys. **68**, 1344 (1978).
[34] I. W. Levin and O. W. Adams, J. Mol. Spectrosc. **39**, 380 (1971).
[35] E. Schweizer, B. N. J. Persson, M. Tüshaus, D. Hoge, and A. M. Bradshaw, Surf. Sci. **213**, 49 (1989).
[36] H. P. Bonzel, Surf. Sci. Rep. **8**, 43 (1988).
[37] S. Efrima and H. Metiu, Surf. Sci. **109**, 109 (1981).
[38] S. Efrima, Surf. Sci. **114**, L29 (1982).
[39] M. Moskovits and J. E. Hulse, Surf. Sci. **78**, 397 (1978).
[40] H. Ueba, Surf. Sci. **188**, 421 (1987).
[41] M. E. Brubaker and M. Trenary, J. Chem. Phys. **90**, 4651 (1989).
[42] R. Disselkamp, H. C. Chang, and G. E. Ewing, Surf. Sci. **240**, 193 (1990).
[43] A. M. Bradshaw, and M. Scheffler, J. Vac. Sci. Technol. **16**, 447 (1979).
[44] A. Liebsch, Phys. Rev. B **17**, 1653 (1978).
[45] T. B. Grimley and S. M. Walker, Surf. Sci. **14**, 395 (1969).
[46] T. L. Einstein and J. R. Schrieffer, Phys. Rev. B **7**, 3629 (1973).
[47] T. B. Grimley, in *The Nature of the Surface Chemical Bond*, edited by T. N. Rhodin and G. Ertl (Elsevier, New York, 1979)
[48] P. J. Feibelman and D. R. Hamann, Phys. Rev. Lett. **52**, 61 (1984).
[49] R. W. Joyner, J. B. Pendry, D. K. Saldin, and S. R. Tennison, Surf. Sci. **138**, 84 (1984).
[50] J. M. MacLaren, D. M. Vvedensky, J. B. Pendry, and R. W. Joyner, J. Chem. Soc. Faraday Trans. I **83**, 1945 (1987).
[51] K. H. Lau and W. Kohn, Surf. Sci. **65**, 607 (1977).
[52] A. M. Stoneham, Solid State Commun. **24**, 425 (1977).
[53] B. N. J. Persson and R. Ryberg, Phys. Rev. B **24**, 6954 (1981).
[54] J. I. Steinfeld, *Molecules and Radiation: An Introduction to Modern Molecular Spectroscopy*, 1st edition (Harper & Row, New York, 1974).